Apoptosis Characterization by Flouro-deoxy Glucose and Intracellular Sodium Distribution Using MicroPET/MRI in PC3 Induced Prostate Cancer in Mice Tumor

Rakesh Sharma[*,**], Richard P.Kline[**],Jose K Katz[**]
[*]Departments of Radiology and Medicine, Columbia University, New York, NY 10032;
[**]Chemical and Biomedical Engineering Department, FAMU-FSU College of Engineering,
Tallahassee, Florida 32310 Email: rs2010@columbia.edu

ABSTRACT

Background: Intracellular sodium (IC) and Flouro-deoxy Glucose **(**FDG) nanomolecules may accumulate in premalignant tumor sites. *Hypothesis:* High FDG and IC accumulation may characterize different tumor stages. *Objective:* To develop rapid noninvasive hybrid microPET/MRI method to characterize PC3 tumor in mice. *Methods:* Sodium MRI by Inversion recovery pulse sequence on 4.23 T MRI and FDG microPET estimated and mapped both IC sodium and FDG at differentiated premalignant and malignant sites in PC-3 cell line induced prostate tumor in mice. These tumor features were confirmed by histology and ss-DNA analysis. *Result:* Apoptosis and other necrosis, carcinoma, sarcoma, neoplasia features were confirmed by immunostaining and MRI/PET imaging showed distinct Na and FDG distribution patterns at these sites as suitable tool for rapid chemosensitivity assay. *Conclusion:* IC sodium indicates apoptosis and FDG pattern indicates higher glycolysis in both pre-malignant and malignant tumors by rapid imaging.

Keywords: *Key words: Nanomolecule mapping, MRI prostate tumor, FDG-PET. sodium MRI*

1 INTRODUCTION

The present study on experimental model of PC3 injected mouse prostate tumor presents possibility of intracellular sodium and glucose uptake by MRI/PET imaging[1,2] and its histoimmunostaining correlates. We attempt in this paper to present PET/MRI techniques to explore the validation and correlation of tumor increased intracellular sodium signal intensity associated with glycolysis, apoptotic cell death by immunostaining as correlates. For better tumor characterization, two issues are important. First, SNR enhancement of sodium MRI signal and PET glucose uptake was accomplished by TMJ coil and hybrid mini imaging system. Second, robust registration and validation of imaging data was correlated with histostaining data.

1.1 High Temperature Superconducting (HTS) TMJ coil for MRI

HTS coil may provide a higher SNR and sensitivity with lower noise imaging of coil. These characteristics indicate low noise temperature and high Q value at low operating frequencies. For small sample size, different variables are interdependent. Following presumptions are: sample resistance is lesser than electrical resistance in coil.

The NMR voltage has an r^2 dependence (where r is linear scale dimension of sample and receiver coil) owing to the r^3 dependence of spin number on volume the coil sensitivity goes as r^{-1}. The noise power of the sample is proportional to ω^2 and to the volume so noise voltage of the sample goes as $(\omega^2 r^3)^{1/2}$. The Johnson noise power of the coil is proportional to the resistance R, which is proportional to the inverse of $\omega^{-1/2}$. So, coil noise voltage varies with frequency $\omega^{1/4}$.

For a series resonant circuit, $Q = \omega L/R$. A high Q leads to reduced Johnson noise as a result of R dependence of the noise power. SNR $\alpha \sqrt{Q/T}$, where T is absolute temperature. YBCO resonator coil at 10 K will yield an SNR gain ~60 relative to copper coil. To achieve SNR gains without significant noise, a coupling approach was used for superconducting resonator as primary and secondary circuits to generate induced NMR voltage or E. At resonance, in primary circuit, inductive and capacitive both reactances cancel out and inductance is real resistance R_p or $Z_p=R_p$. The secondary circuit has low capacitor. The effective impedance in secondary circuit is $(\omega M)2/Z_p$. These both circuits experience mutual inductance M between two resonant circuits. By adjusting both resonators, M can be large enough. SNR depends on parameters of noise voltage generated by coil, body and preamplifier as following:

$$\text{SNR} \alpha E/\sqrt{R_p} \text{ (for primary circuit)} \quad (1)$$

$$\text{SNR} \alpha (\omega ME)2/R_p[(\omega M)2/R_p]1/2 = E/\sqrt{R_p} \quad (2)$$

$$\text{SNR} = \frac{B_1}{\sqrt{R_c T_c + R_s T_s}} \quad (3)$$

where R_c is resistance of coil and R_s is resistance of body surface; $\sqrt{R_c T_c + R_s T_s}$ is noise voltage.

Noise source and quality factor, Q: Coil resistance R_c and body resistance R_s may be defined as:

$$R_c = \omega L/ Q_o \quad (4)$$

where L coil inductance, Q_o is quality factor of unloaded RF coil and Q_L loaded RF coil.

$$R_s = \omega L/ Q_L - R_c \quad (5)$$

1.2 The mini-PET/MRI system

A device was used as reported earlier [3]. It fits inside the top of the magnet, is shown in Figure 1, together with the position of the MRI probe and animal, which fits into the bottom of the magnet. A MRI coil completely surrounds the animal; thus the ^{23}Na MRI signals observed originate from the whole tumor.

The PET scanner fits over the top of the MRI probe such that a single, midventricular PET scan is obtained. For the pilot experiments, tumors were scanned earlier separately for MRI and PET scans as described earlier [1].

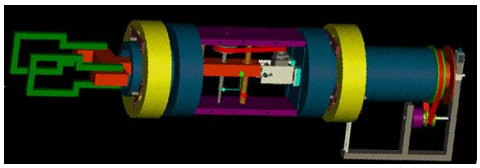

Figure 1: Micro PET/MRI system for data acquisition.

1.3 AIR and MI registration algorithms

The AIR algorithm uses a correlation cost function and a ratio cost function. The MI algorithm uses a number of subsampling steps: 884, 442, 221, or 111 (XYZ subsampling). Prealignment by manual reorientation places the volumes within the algorithm's "capture" range. Volume trimming removes image points not common to both PET and MRI data sets. A rigid geometric transformation (six parameters) without smoothing in AIR and MI algorithms used the convergence optimization method. However, singular value decomposition (SVD) algorithm estimates the registration errors to give "perfect" registration transformation matrix. This transformation was applied to a set of points spaced in and around the mouse tumor. The SVD-transformed set of points was then retransformed with the inverse of the transformation matrix arising from the multimodality registration. The mean Euclidean distance between these final points and the maximum distance between these points measured the registration accuracy and the "functional performance" of both algorithms.

2 MATERIALS AND METHODS

PC3 induced mouse tumor was propagated as reported earlier [3]. For validation of PET image intensities, biotransformation was optimized and a criterion was developed for pre- and post-malignancy by histology. For correlation, regression analysis was done using imaging, histology and immunostaining data from PC3 tumor imaging of 24 hours post- taxotere treatment. Apoptosis indices (appearance of beaded nuclei) were measured by pentachrome, feulgen and ss-DNA antibody. Sequential scanned MRI (1 mm slice) and dynamic PET images over tumor area were acquired. Biotransformation data was acquired at different 4 time points of 10, 20, 50, 80 minutes after injection of FDG. In serial images, the correction factor was set at biotransformation rate after 50 minutes to achieve isointense tumor images for registration with MRI images. Further, image data were corrected for uniformity, sensitivity, attenuation and images were reconstructed using Hanning filtered convolution back-projection with cut off value of 1.0. The PET images were fused with transaxial MR images and using MEDEX software drew volumetric region of interest.

For validation of MRI signal, different TE and TR were plotted for images of two tubes with NaCl and agarose plus NaCl solutions [3]. Imaging and histo-immunostaining data was used for histology. For, image processing and statistical correlation, Optimas 6.5 and PRISM 3 were used. Tumor pre-malignancy criterion was developed based on MRI and PET signal intensities and histology features in tumor by correlation analysis.

3. RESULTS

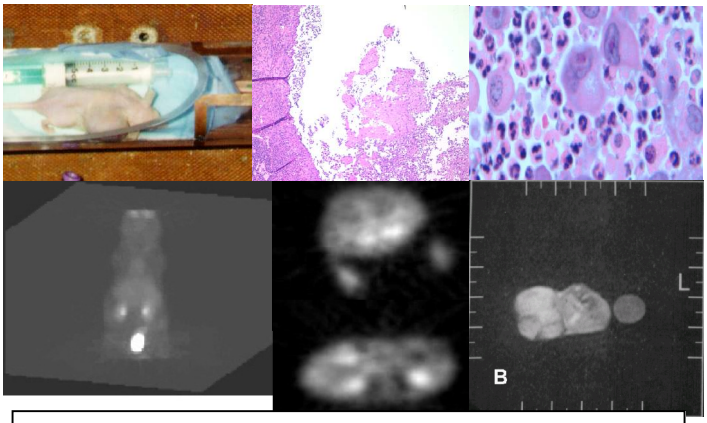

Figure 2: Top row: A PC3 explanted tumor, histology with apoptosis nuclei(on right). Bottom row: A dynamic 3D whole mice PET, transaxial sections of tumor(middle) matched with sodium MRI of tumor(right). Tumors appear brighter.

3.1 SQ and TQ sodium image intensity variants

SQ and TQ images of a large tumor showed high sodium signal intensity in tumor compared to normal tissue in the Na images. However, there was a higher contrast between tumor and normal tissue in the TQ image compared to the SQ image. It was due to higher sodium sensitivity to TQ NMR. Images are shown for PC3 tumor in vivo, both at baseline apoptosis rich tumor and 18 hours after i.v. injection of 1 mg of taxotere in the femoral vein. SQ line profiles did not significantly vary after drug administration. There was a substantial increase in the TQ line profile. These results indicated that $[Na]_i$ increased due to chemotherapy based on SQ and TQ imaging. Using high temperature super conducting coil, increased signal-to-noise ratio in TQ Na imaging by a factor of 10 and decreased imaging time by, a factor of 100.

3.2 Monitoring of therapeutic response by tumor signal intensity in IR Na image

The technical use of SQ and IR sodium images were evaluated visually for diagnostic accuracy and its value in drug therapeutic monitoring. Taxotere enhanced intracellular sodium up to a certain peak time and later the effect was reversed. On histology sections from same tumor regions, mitotic figures were inversely correlated.

Sodium MRI signal Intensity		PET SUV	Histology	Tumor characteristics
SQ Na MRI	IR Na MRI		Tumor features	Tumor stage
				Pre-malignant stage:
isointense	++	+	Viable	Intraductal proliferation,
dark/gray	+	+	Active necrosis	ductal hyperplacia, apoptosis
gray	++++	+++	Early apoptosis	**Malignant** stage:
+++	bright/gray	+	Late apoptosis	Carcinoma (papillary; invasive comedo and cribriform)
++++	dark		Cyst	sarcoma, neoplasia

Table 1: Relationship of sodium MRI signal intensities and glucose uptake by PET SUV with histology features and tumor cytomorphology characteristics.

3.3 Validation and selective acquisition of intracellular ^{23}Na by use of inversion recovery (IR)

To visualize both PC3 tumor morphological details, both SQ and IR sequences were applied. The effects of varying inversion time (TI) and echo time (TE) were indicative of the intracellular sodium signal dependence on these MRI scan parameter values. The tumors were comparable on sodium images with phantom images.

3.4 Apoptosis index and MRI/PET association with premalignancy

The tumor histology features displayed the association with increased sodium MRI signal intensities and increased glucose uptake (SUV) values or glycolysis rate in intact prostate tumors as shown in Table 1.

4 DISCUSSION

Apoptosis is controlled and programmed cell death in premalignant tumors. It is observed as active proliferation, viable cells, reduced mitotic bodies with beaded nuclei and membrane 'blebbing'. These changes can be confirmed by histo-immunostaining, ss DNA mapping, pentachrome, KI67, feulgen and Annexin V staining. The apoptosis appears to affect the membrane transport associated sodium pump activity. Presumably, indirect relationship of intracellular sodium and apoptosis may provide rapid imaging capability to define or detect premalignancy in time dependent manner. Mice model of explanted prostate tumor serves as rapid chemosensitivity drug assay. Premalignant and malignant lesions in mice injected with PC3 at 50 days of age showed various similarities such as biological, morphological, and molecular properties with many characteristics observed in the human disease process that closely mimic with human prostate cancer.

The single-strand DNA monoclonal-based method enhanced the power of detection for different stages of apoptosis in tumor. Spatial resolution of the image (~1 mm within each slice) varies with enhanced signal intensity, and apoptotic-localized region or an increased density of early apoptotic cells. Apoptosis ends with complete DNA fragmentation and loss of cell nuclei after long time period. Hence, the absence of an IC Na MR signal intensity in late apoptosis can be explained by the loss of bound sodium in prostate tumor that the average IR-sodium intensity increase was smaller at 48 hours than at 24 hours. The pixel intensity histogram pattern characteristically showed distinct main peak of S-DNA predominantly neoplasm. CAS 200 method was efficient in distinguishing cell cycle phases as S, M peaks.

The results demonstrate the possibility of detection of apoptosis and possibly the neoplasia *in vivo* using MRI and PET. We believe that Taxotere administration may lead to significant IC sodium contrast increases in tumor regions rich with apoptotic cells. The MRI technique can detect apoptosis at an early stage in the process and has advantage over MRS and other radionuclide approaches with high spatial resolution. The PET suggests the instant glucose uptake in tumor initial stages by 3D dynamic visualization. Like H & E staining, MRI can detect the tumor necrotic cells with ruptured plasma membrane making access of intracellular sodium or staining material on inner leaflet. However, the detection of slow cell death by MRI or PET appears as challenge. This sodium MRI technique is one of the growing MRI method that could allow the investigation of cell physiology in intact tumor. The nanoscale measurement and distribution of intracellular sodium may be performed by electron beam computer tomography (EBCT) and high resolution FDG-PET by using customized flow algorithm.

REFERENCES

[1] PK Marsden, D Strul, SF Keevil, SCR Williams, D Cash. Simultaneous PET and NMR. Br J Radiol 2002;75:S53–S59.
[2] Y. Shao, S. Cherry, K Farahani, R Slates, RW Silverman, K Meadors, A Bowery, S. Siegel, PK Marsden, PB Garlick. Development of a PET detector system compatible with MRI/NMR systems. IEEE Trans Nucl Sci 1997;44:1167–71.
[3] R Sharma, P. Esser, H. Van Heertum. AACR conference on Molecular Imaging in Cancer: February 2002 Orlando, Paper A-3.